ADVANCED NUMERICAL SIMULATIONS ON STRUCTURED GRIDS FOR TRANSPORT AIRCRAFT, USING AN EFFICIENT OBJECT ORIENTED SOLVER.

L. BARRERA - Airbus France, Fr,
Ch. BENOIT, M.-C. LE PAPE, R. HOUDEVILLE, J. PETER - ONERA, Fr,
J.-C. JOUHAUD - CERFACS, Fr

Keywords: *Navier-Stokes, Object-Oriented, Chimera, AMR, Wall laws, Ground effect*

Abstract

This paper presents the most recent simulations made at Airbus France, using advanced structured grids techniques available in the new generation CFD solver elsA. Three aircraft applications have been carried out in order to show the potentiality of the new functionalities applied on complex configurations. First, a Chimera calculation was performed in order to assess ground effect prediction as an alternative to the panel method currently used today. Then, a Multigrid Adaptive Mesh Refinement strategy was applied on an isolated swept wing to evaluate accuracy improvements on shock wave prediction. Finally, recent improvements achieved in the wall law function were tested on a Navier-Stokes engine/airframe configuration and compared to a classical low Reynolds turbulence modeling approach.

Nomenclature

ρ	density
α	angle-of-attack
M_o	free stream Mach number
$h_{landing}$	minimum height of aircraft gravity center at landing
h	height of aircraft gravity center
H	$h- h_{landing}$: relative ground effect height
C_{Lo}, C_{Do}	lift and drag coefficients at free-stream conditions
b	half wing span
B	total wing span
y_{+1}	first wall cell size in wall units

1 Introduction

Numerical methods are now widely used throughout the aircraft design process. In particular, Airbus intensively uses CFD within the scope of its responsibilities in all projects and programs for the design and optimization of aerodynamic shapes.

Moreover, as a complement to wind-tunnel tests and semi-empirical methods, CFD is more and more used in the assessment of aerodynamic data for performance, loads and handling qualities.

Today, most of our Euler and Navier-Stokes calculations are carried out on coincident structured meshes. In order to optimize design cycles and to fulfil the new needs and constraints relative to aerodynamic data generation, new numerical methods have been investigated:

- Chimera technique to reduce time spent in mesh generation and to allow geometrical parametric studies without creating new meshes.
- Multigrid Adaptive Mesh Refinement to improve result accuracy without downgrading computing performance.
- Turbulence wall law models to improve computing performances and convergence rate without downgrading accuracy.

2 elsA solver

With the objective of federating all national research teams and taking advantage of older functionalities implemented in separate CFD codes, ONERA has been developing a new generation solver called elsA since 1996, in co-operation with CERFACS. It has been designed according to an Object Oriented design method and it is mainly coded with C++ language, thought the most CPU-expensive loops are coded with Fortran language for better numerical efficiency. This innovative approach leads to more upgradeable and inter-operable aerodynamic functions, and thus contributes to better integration of different development [1].

The main features and numerical functions of elsA are listed below:

- cell centered code dealing with structured meshes.
- no ghost-cell to ensure the connection between domains (connecting data are temporary)
- classical central and upwind fluxes for Euler model (centered flux with scalar or matrix dissipation, Van Leer flux, Roe flux)
- viscous flux computed from cell -centered evaluations of velocity and temperature gradients
- classical algebraic and transport equations turbulence models (all of them following Boussinesq's assumption). Similar discretization for the terms of the turbulence models and those from the mean flow system.
- three classical mechanical formulations (absolute variable/absolute or relative frame, relative variable/relative frame).
- Runge-Kutta or backward-Euler time integration for steady flows, dual time-stepping for unsteady flows.
- various multi-domain/ convergence acceleration strategies : global multi-grid, local multi-grid and adaptive mesh refinement and chimera.
- mesh deformation
- low-speed formulation

We describe below more precisely the very recent developments, which were used in this study for aircraft applications.

2.1 Chimera grids

2.1.1 Chimera principle

The Chimera method is based on an overlapping grid technique [2]. Its principle is to mesh independently different bodies and then to take into account interactions between the different components by interpolations. More precisely, on the one hand the mesh areas overlapped by bodies are not computed by the solver and body influence comes from a cell crown around the body; on the other hand, domain influence goes through outflow boundaries. This technique allows the body to be meshed quite independently, meshes must only sufficiently overlap to enable interpolations. Meshes can also be re-used for different relative positions. In elsA, the interpolation is piecewise linear by tetrahedron, each cell being divided into 24 tetrahedrons. Bodies are modeled by a great number of parallelepipeds. Interpolation cell research becomes efficient by using a preconditioned cartesian grid and other acceleration techniques to find the interpolation tetrahedron [3],[4]. In order to reduce overlapping constraints and prevent some points from becoming orphan, extrapolation from neighbor cells is allowed; the numerical scheme is also degenerated on overlapping boundaries and around bodies, then interpolation crown and boundaries have a width of one cell [5].

2.1.2 Implementation in the elsA software

In the elsA software, using Chimera consists in defining overlap boundaries and body surfaces. Our implementation can be used for steady and unsteady flows (even with moving bodies) and with various turbulence models. However, using it in conjunction with the Multigrid acceleration technique is not yet available.

2.2 Adaptive Mesh Refinement

2.2.1 Hierarchical Grid Structure

The Multigrid AMR algorithm consists in a sequence of integration on different grid levels ($0 \leq l \leq l\max$). A grid G_l is required to be union of sub-blocks in which the same discretization procedure is applied:

$G_l = \cup_k G_{l,k}$, where $G_{l,k}$ are elementary sub-blocks.

The hierarchical grid structure respects the "properly nested property" [6] which is based on the following three rules:

(1) $\forall l \ 0 \leq l \leq l\max$, $G_l \subset G_{l-1}$, inclusion of underlying grids ;

(2) $G_{l,k} \cap G_{l,h} = \varnothing$ if $k \neq h$, no overlapping ;

(3) adjacent cells of G_l must only belong to the level $l-1$, except for external or wall boundaries.

The first rule ensures the successive grids nesting, i.e. the gradual basic mesh enrichment with finer and finer meshes. It means (with the third rule) the recursiveness of the method.

The second rule is a standard choice, which prevents overlapping, which is very expensive in computation time and memory storage.

The third rule enforces a strict inclusion and leads to a gradual distribution of refinement zones from the coarsest to the finest. However, it permits a finer and finer refinement near the solid boundary.

2.2.2 Combining AMR and multi-grid methods

The classical AMR method, i.e. the method developed by Berger & Collela [7] is valid only for unsteady flows. Indeed, it is no longer valid for steady flows because convergence on the hierarchical mesh is not guaranteed.

Here, we have developed a local 3D multi-grid algorithm for embedded meshes called *Multigrid AMR*. Based on the multi-grid approach, this technique [8] not only couples the different levels of grid but also accelerates the convergence to steady state.

It is based on a local forcing function, which allow a local formulation of Jameson's Full Approximation Scheme [9]. This local forcing function modifies coarse block residuals by constructing so-called composite residuals.

2.2.3 Automatic Grid Adaptation

Once the aerodynamic solver is able to treat local refined meshes, it is important to develop a specific tool for an automatic calculation of sub-block location, based on aerodynamic user criteria. Since 1994, Airbus has been developing such a tool called MBREF. It is interfaced with our in-house data base environment DAMAS (DAta for Meshes and Aerodynamic Solvers) and can be divided into the following stages:

- compute a sensor (between 0 and 1) on the all volume cells. Today, two Euler sensors respectively based on simplified density and pressure gradients are available.

$$s = \frac{s_{ijk}}{\max_{doms}(s_{ijk})}$$

$$s_{ijk} = \max\left(\Delta\overline{\rho}_{i+}, \Delta\overline{\rho}_{i-}, \Delta\overline{\rho}_{j+}, \Delta\overline{\rho}_{j-}, \Delta\overline{\rho}_{k+}, \Delta\overline{\rho}_{k-}\right)$$

$$\Delta\overline{\rho}_{i+} = \frac{|\rho_{i+1} - \rho_i|}{\min(\rho_{i+1}, \rho_i)}.....$$

- flag the cells satisfying a criteria, usually

$$s \geq s_{threshold}$$

- compute sub-block locations according to the "Grouping/Clustering" algorithm defined by Quirk [6]. A constraint on minimum flagged cells in a sub-block is defined by means of a creation ratio.

$$\left(\frac{N_{flaggedcells}}{N_{total}}\right) \geq C_{flag}$$

- create sub-blocks in the data base taking care to project the new surface points onto the CAD shape (stored in data base).

In practice, the user can manage the refinement strategy:

- increasing the flag threshold value $s_{threshold}$ to be more selective about regions to refine.
- increasing the creation ratio C_{flag} to obtain a larger set of sub-blocks fitting the flagged structures well

2.3 Wall laws

In a turbulent boundary layer, the mesh must be extremely refined at the wall in order to correctly simulate the strong velocity gradients in the wall region, as well as the skin friction coefficient and other turbulent variables. More precisely, the height y^+_1 of the first cell on the wall (in wall units) is usually fixed around 0.3-1.0 depending on the turbulence model. Such a constraint leads to large mesh sizes, low time steps and large aspect ratio of the cells near the wall, which are damaging for accuracy and convergence of the numerical scheme. A very efficient way of improving consists in applying the wall law on the first cell the size of which can be much larger than $y^+_1 = 1$.

At the walls, a no-slip condition is still used. As the sizes of the adjacent cells are large, in the order of 50 to 100 in wall units, the shear stress τ and the heat flux q representing the diffusive flux densities must be obtained using a particular treatment. The velocity profile in the wall region $\overline{u}^+ = f(y^+)$ is assumed constant, with f a combination of linear and logarithmic functions. $\overline{u}^+$ is the Van Driest transformed velocity taking the compressibility effects into account. Instead of using an explicit temperature profile in the wall region, a temperature-velocity relationship is preferred. It is deduced from the integration of the total enthalpy equation by neglecting the advection terms.

The wall treatment is straightforward. Knowing the velocity from the Navier-Stokes solution, $\overline{u}^+$ is obtained from the Van Driest transformation and the velocity-temperature relationship. The velocity wall law gives the shear stress, which is assumed constant in the direction normal to the wall. To extend the wall treatment to separated and 3D flows, the wall law is expressed in a reference frame defined by the velocity direction in the cells adjacent to the walls. Such a treatment is not in contradiction with the fact that the log law does not exist in separated regions. Actually, in these regions τ_w remains small and therefore y^+ also, leading to the use of the linear part of the velocity profile. This is equivalent to computing the velocity gradient over two points instead of three for the ordinary cells.

As far as the transport equations of the turbulence models are concerned, k is imposed at the center of the cells adjacent to the walls using the Bradshaw hypothesis. The second turbulent variable is deduced from analytical relation and is also imposed in the cells adjacent to the walls. For the k-ω model, the characteristic length scale of the Chen model [10] is used for the specific dissipation ω. For the k-l model, l is proportional to the wall distance. For the Spalart-Allmaras model, $\tilde{\nu}$ is imposed by using the closure relations of the model, the velocity profile and a mixing-length formulation for the eddy viscosity [11].

3 Aircraft applications

3.1 Ground effect prediction using Chimera grids

3.1.1 Introduction

When an aircraft comes near the ground, its aerodynamic characteristics are modified. Ground effect especially influences longitudinal coefficients: lift, drag and pitching coefficients. Consequently, aerodynamic coefficient variations must be correctly assessed before integrating them in the control laws modeling, especially for automatic landings.

Ground effects are usually broken down into 2 contributions: aircraft without tails and tails contributions. The current study is limited to drag and lift variations on an aircraft without tails.

When the aircraft comes down to a minimum "landing" height $h_{landing}$, experimental measurements as well as numerical computations show:
- a decrease of induced drag
- an increase of lift in most cases. However, the trend can be reversed at low heights, at high angle-of-attack and in high lift configuration

The induced drag reduction can be explained by the influence of the "symmetric" wing tip vortex, which turns in a direction contrary that the basic plane vortex, damping the original vortex. The magnitude of the reduction mainly depends on the full aircraft span B and the absolute wing height.

Among many drag reduction factor modelizations for simplified unswept wings, Laitone suggested a correction of MacCormick formulation, which gives better values for low height [12]:

$$\Phi = \frac{C_{Di}}{C_{Di\infty}} = \frac{\left(1 - (2/\pi) + (16h/\pi B)^2\right)}{\left(1 + (16h/\pi B)^2\right)} \quad (1)$$

The ground effect on lift results from two opposite effects:

- for low angle of attack and high height, the presence of "symmetric" wing vortex induces an upstream perturbation speed and vertical perturbation speed at trailing edge. Considering the small disturbances approach, it can be shown that lift increases.

- for high angle of attack and low height, the ground reduces the effective angle of attack (channeling air flow). Flow is accelerated in the convergent duct generated by wing and ground, and so the wing is sucked downward : the lift decreases

The second effect explains a sudden decrease of lift for low height and high angle-of-attack, sometimes leading to negative lift variations. Moreover, it was shown that this phenomenon is all the more visible as the high lift devices are deployed [15]. Similar behavior was also shown on a cambered single element wing, as regards the variation of the downforce (in the racing car context) as a function of height and angle-of-attack [12].
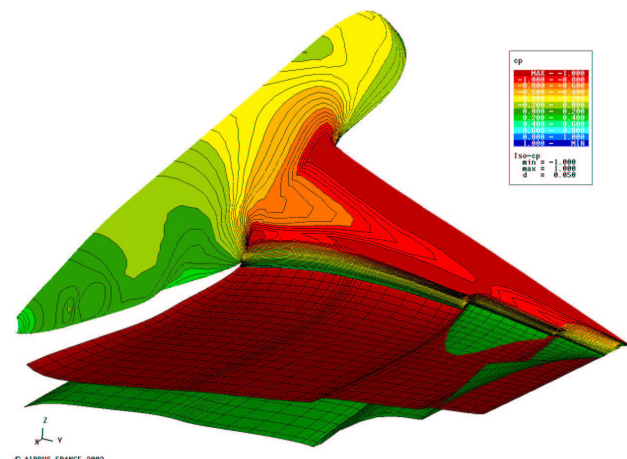
3.1.2 Panel method

Today, the most commonly used numerical method at Airbus for ground effect prediction is based on a source/vortex panel method, completed with a vortex sheet balancing

algorithm. An "envelope" shape (no slot effects) approximates wing geometry and no viscous effects are taken into account [14].

This method is very efficient (with respect to CPU time) and useful because:

- surface meshes are generated rapidly

- there is no need to generate multiple meshes for different aircraft heights. Horizontal symmetry plane condition is only introduced in the influence matrix coefficients.

- the calculation itself is very quick (half an hour on a CRAY J916)

- during the post-processing stage, induced drag can be directly computed from vortex values given by the solver.

Calculations were performed on the simplified Airbus fuselage/ envelope wing configuration at $M_o=0.3$. A parametric study was conducted varying both the angle-of-attack (4°, 7° and 10°) and undimensionned height (H/B=0%, 5%, 10%…. 100%), where $H = h - h_{landing}$ is the relative height with respect to landing height (full ground effect). Figure 1 shows a general view of the configuration with the initial and final balanced wakes. The mesh contains 6000 panels (4000 on skin, 2000 on skeletons and wakes)

**Figure 1 - Panel method on Airbus configuration
M=0,30 - α=10 °H/B= 0%**

3.1.3 Chimera method using elsA

Even though panel method is very efficient, it has many drawbacks for future applications. Wing geometry has to be

simplified because real multi element airfoils cannot be correctly simulated by inviscid methods, even by coupled methods. Moreover, in the presence of tails, there are strong viscous interactions with rear fuselage and wing wake.

Therefore, it was natural to simulate this configuration with Euler and RANS solvers. Unfortunately, within a classical multi-block approach, the mesh had to be generated for every height and every angle-of-attack. In order to avoid this repetitive mesh generation, a Chimera simulation can be carried out in which the classical aircraft mesh moves into a "ground" mesh (cartesian grid) at different heights and angles-of-attack.

ElsA calculations are performed with the Euler model on the same fuselage/wing configuration studied with the panel method. The goal of this study is to show that the Chimera model is able to simulate the same ground effect as the panel method, and prepare the way for Navier-Stokes calculations on multi element wing configurations.

Figure 2 shows a general view of the Euler mesh used for the Chimera simulation. The original aircraft mesh is made up of 24 structured blocks (960 000 nodes). It is immersed in a single ground block (30 000 nodes) as illustrated in the y- symmetry plane
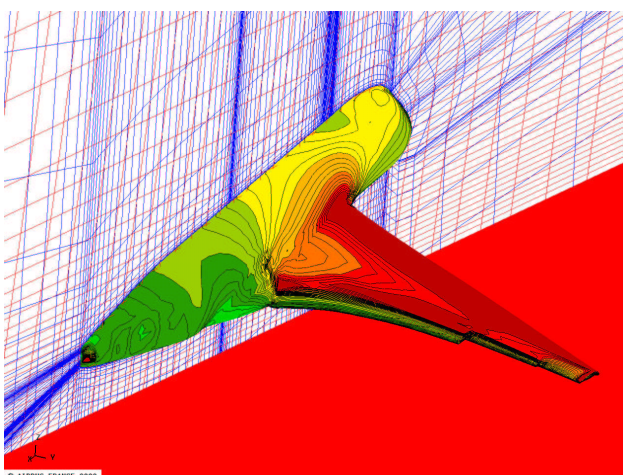

Figure 2 - Chimera method on Airbus configuration M=0,30 - α=10 °H/B= 0%

3.1.4 Numerical results

A qualitative comparison of Figure 1 and Figure 2 shows a similarity between pressure fields on wing and fuselage.

Due to low values of the lift variations we are looking for, the convergence of Chimera calculations must be carried far enough, until complete stabilization of the lift coefficient. For each couple of height and angle-of-attack, 4000 implicit cycles were necessary, because the association with multigrid acceleration is not yet available.

Lift and drag coefficients were computed in the same way for the two calculation methods, by integrating pressure coefficients on the aircraft skin. All the results are summarized in Figure 3. Lift and drag variations are non-dimensioned with respect to values obtained without ground effect. Chimera Euler results are plotted using filled symbols while the curves refer to panel the method parametric study.

Ground effect on lift has three different behaviors depending on angle-of-attack:

- at α=4°, lift always increases when height decreases.
- at α=7°, lift begins to increase when height decreases, then it decreases near the ground while remaining positive
- at α=10°, lift begins to increase slightly when height decreases, then it strongly decreases near the ground even becoming negative

Chimera calculations were only performed at 2 heights for each angle-of-attack (full ground effect and 10% of total span height). The Euler Chimera results are in accordance with the 3 different behaviors as regards the lift, even if absolute values slightly differ from panel method results.

Ground effect on drag has the same behavior for the three angles of attack. Chimera results are very close to the panel results. Due to low speed conditions and assuming that the ground has no effect on viscous drag, the

decrease only affects the induced drag. The panel method post processing confirms this assumption insofar as same drag ground effect was found using near field approach (pressure integration) and far field approach (Trefftz plane method based on wake vortex values)
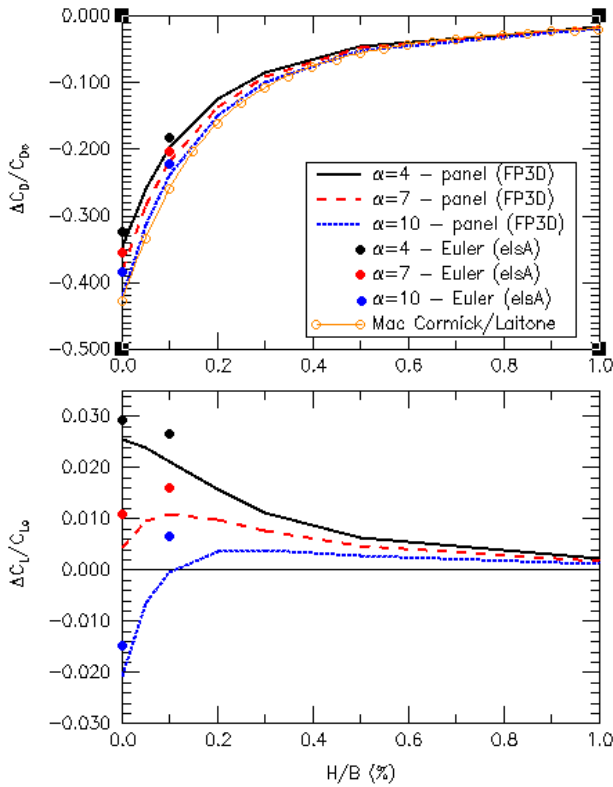

Figure 3 - Ground effect on lift and drag

As an indication, the ground effect modelization from (1) has been also plotted, even if the wing has a sweep and dihedral angles. The minimum height h/B corresponding to landing was chosen considering the wing tip height, where the strongest wake vortex appears.

3.2 Improving drag breakdown accuracy using Multigrid Adaptive Mesh Refinement

3.2.1 Introduction

The correct prediction of the wing shock wave pattern is of the utmost importance for drag prediction. With current methods, coincident meshes have to be considerably refined before obtaining mesh convergence with respect to wave drag.

In order to improve accuracy while keeping reasonable mesh size, there are two approaches to adapt structured meshes and refine them around flow patterns. The first method simply moves nodes keeping the same blocks topology, while the second method introduce new blocks for local mesh refinement.

The second approach was tested in the current study. Starting from a coarse mesh, different levels of sub-blocks (locally refined blocks) were automatically computed and introduced using the MBREF tool.

3.2.2 Configuration description

To illustrate this potential gain, a simulation was carried out with the Euler model on a swept wing configuration at M_o=0,80 and α=2,2°. At this flow condition, a swept shock wave appears along the wing, and a smooth supersonic compression appears in the inner wing creating a "lambda" pattern (see Figure 4). A reference fine mesh containing $1,6.10^6$ nodes was unrefined along each direction, to generate both a medium mesh (1 node out of 2: 210.000 nodes) and a coarse mesh (1 node out of 4: 28.000 nodes). The fine mesh is illustrated in Figure 4 : two blocks are arranged around the wing using a C-O topology.
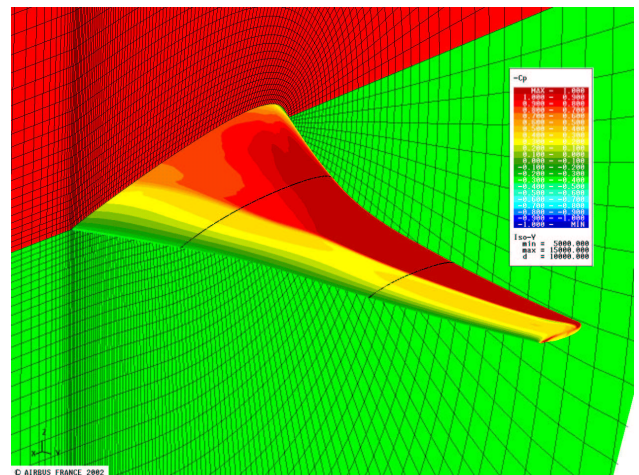

Figure 4 - AS28 wing - Euler Mesh - M=0,80 α=2,2°

The goal of this study is to obtain an equivalent accuracy to fine mesh, on a local refined mesh obtained by introducing 2 levels of refined blocks on the coarse mesh.

As mentioned in paragraph 2.2.2, MBREF mainly depends on 3 main user parameters: the

sensor, the creation ratio and the flag threshold In the present study the first two parameters were fixed: density sensor and C_{flag}. Then, we studied the influence of flag threshold on the automatic introduction of two sub-blocks.

3.2.3 Numerical results

Starting from the coarse mesh, two different mesh refinements were studied, varying the flag threshold involved in automatic introduction of two levels of sub-blocks:

- Refinement A : flag thresholds used for the two levels are identical: s_{lim1}=5% s_{lim2}=5%
- Refinement B : level1 flag threshold is lower than level2: s_{lim1}=2% s_{lim2}=8%

Refinement A creates 2 sub-blocks at level1 and 5 sub-blocks at level2. The refined meshes are shown on Figure 5.
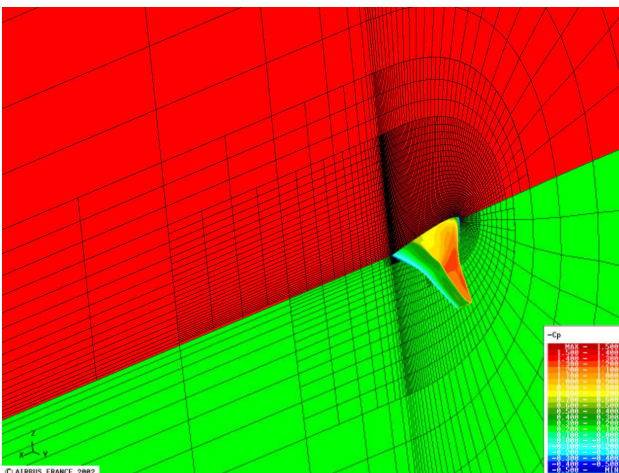
Figure 5 - Two level refined topology A

Pressure distributions are plotted on Figure 6 along sections illustrated in Figure 4, and compared to results obtained on fine mesh. Pressure peaks at leading edge and shock wave sharpness are equivalent to fine mesh, but the shock wave is located slightly upstream. This difference is probably induced by an insufficient extension of the first refinement level.

In order to verify this assumption, a second refinement B was tested, trying to be less selective at level1 and more selective at level2, to obtain roughly the same mesh size. It creates 2 sub-blocks at level1 and 6 sub-blocks at level2. The refined meshes are shown in the Figure 7.
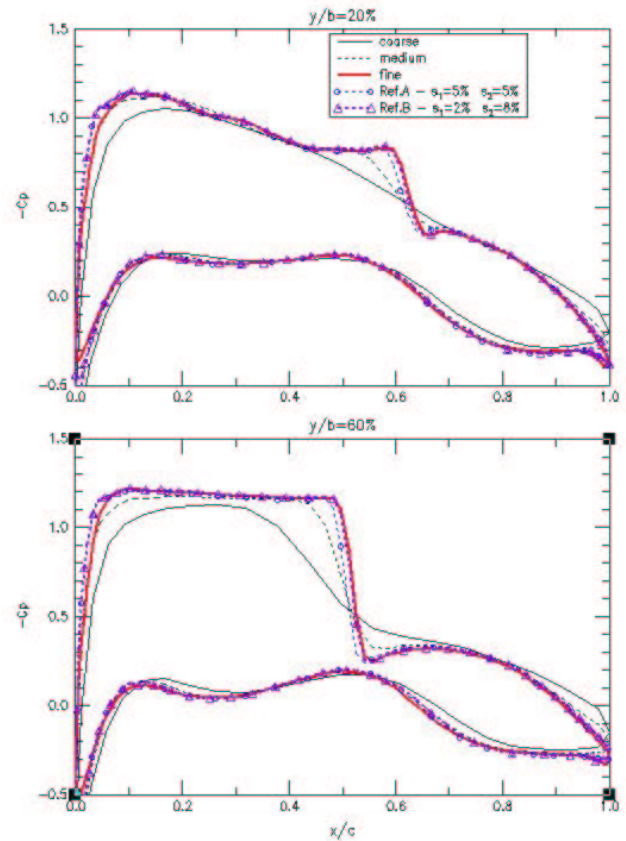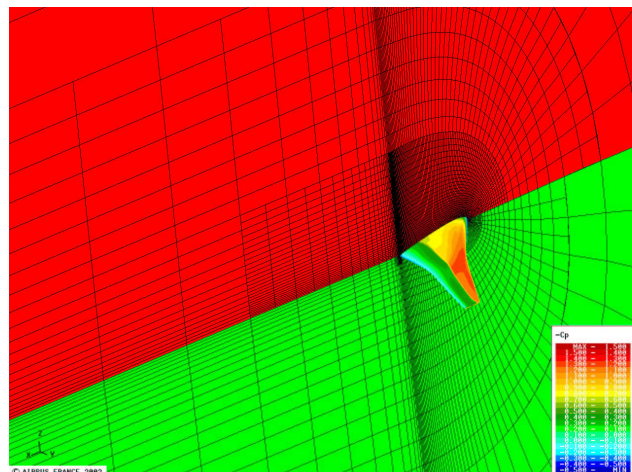

Figure 6 - Wing pressure distribution

Figure 7 - Two level refined topology B

With this new refinement, the shock wave is now located very close to the fine results (see Figure 6). However, pressure comparison matching is often an insufficient argument for accuracy comparison, especially if designer study focuses on drag breakdown.

Thus, drag breakdown post processing was carried out on all fine, medium, coarse and locally refined calculations, using the FFD40

tool which was developed by ONERA in co-operation with Airbus France [16]-[17]. A specific development was necessary, so as not to take the masked cells on coarse and medium meshes into account during drag integration. As illustrated in Figure 8, the first refinement is insufficient to predict shock wave drag (~ 4 drag count error) while the second refinement provides an error less than 1 drag count.

This application shows that an equivalent accuracy can be obtained using a locally refined mesh, compared to a fine mesh roughly three times as big. Thus, the CPU time and memory efficiencies can be reduced by a third, insofar as AMR treatment cost is negligible compared to computation cost.
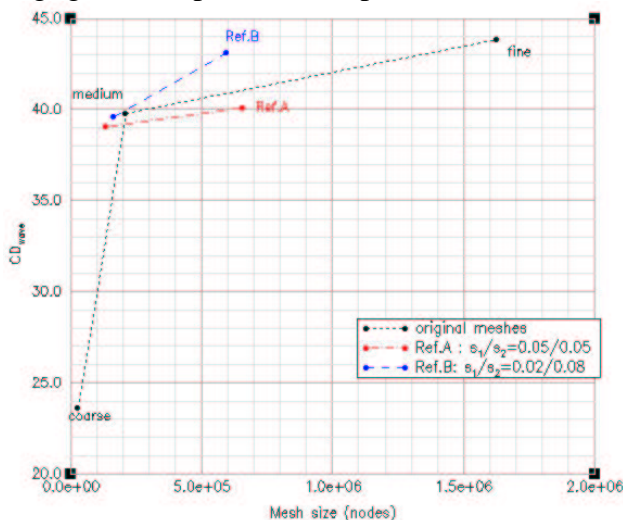

Figure 8 - Wave drag for initial meshes and local refined meshes

3.3 Efficient engine/airframe integration using wall laws for Navier-Stokes simulations

3.3.1 Introduction

Turbulent Navier-Stokes simulations around complex geometries, such as power plant /airframe configurations are now widely used at Airbus for the design and optimization of pylon and nacelle shapes. Unfortunately, the current meshing approach leads to big meshes and expensive calculations due to the severe boundary layer refinement near the wall, which is necessary for the most usual low Reynolds turbulence models. For this reason, some geometries such as flap track fairing and wing

tip fences are often not taken into account in Navier-Stokes calculations.

In addition to the increase of the mesh size, the extreme refinement in the vicinity of the wall around wing, pylon and nacelle bodies has other drawbacks:

* it spreads out over the whole domain calculation, unnecessarily covering some regions with low flow gradients
* the convergence rate can be slowed down due to small time steps
* it induces other refinements on neighboring domains in order to ensure cell size continuity (rear surfaces on thick trailing edges)
* some precision problems may be found during mesh generation, and when meshes are modified during shape optimization cycles or structure coupling cycles.

The successful validation of wall laws on 3D configurations, even in the presence of separated flow, has been shown recently [11] with four popular turbulence models (k-ω, k-ε, k-l and Spalart Allmaras). The use of a wall law turbulence model allows a considerable decrease of the mesh size (about 1/3), thanks to a larger wall cell size y^+_1=50, instead of classical value y^+_1=1. Moreover, the increase in the wall cell size often leads to a better convergence rate.

The aim of this application consists in computing a complex power plant/airframe configuration using both low Reynolds turbulence model and wall law model, in order to show that Navier-Stokes calculations can be carried out at lower cost, with the same accuracy.

3.3.2 Configuration description

The configuration is composed of a swept wing section between two vertical walls, equipped with a pylon and a powered nacelle.

The original mesh is made up of 27 coincident structured blocks. The mesh used for the wall law calculation is then derived by merging the first 9 cells near the wall, according to recommendations specified by ONERA. In this way, mesh size decreases from $2,25.10^6$ nodes to $1,64.10^6$ nodes.
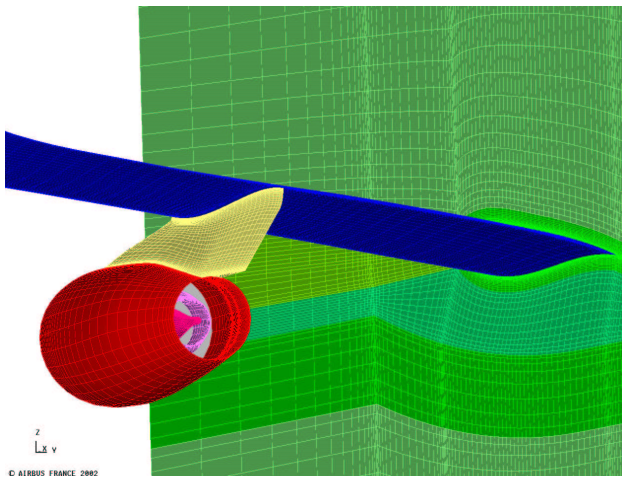
Figure 9 - S3Ch powerplant configuration

The calculations were made using experimental corrected values $M_o=0,82$ - $\alpha=1,56°$ - $Re_1=12,4.10^6$ (per unit length) and ignoring upper and lower wind tunnel walls. Engine TPS (Turbine Powered Simulator) operating conditions are simulated by the following numerical boundary conditions:

- subsonic injection at fan and core exit : $Pt_{fan}/Pt_o=1,49, Tt_{fan}/Tt_o=1,16$, $Pt_{core}/Pt_o=1,78$, $Tt_{core}/Tt_o=0,64$
- constant pressure at fan face: $p_{fan}/p_o=1,43$

3.3.3 Wall law boundary condition effect

The Wilcox k-ω turbulence model has been used in the wall law calculation associated with the Jameson scheme for the RANS system ($\kappa_2/\kappa_4=0,5/0,016$) and a second order Roe scheme for the turbulence equations. Time integration uses a backward Euler scheme coupled with LU implicit and multigrid acceleration techniques on 2 grid levels.

The Residual convergence history in Figure 10 shows that both calculations using wall law mesh and refined boundary layer mesh converge in 1000-1500 cycles, with four orders of magnitude reduction on the density residual and complete stabilization of aerodynamic coefficients. The residuals were divided by the initial values and the final values were subtracted from the aerodynamic coefficients. The aerodynamic coefficients in the wall law calculation are stabilize faster even if the residuals have higher values. Running on four processors in parallel mode, the calculation

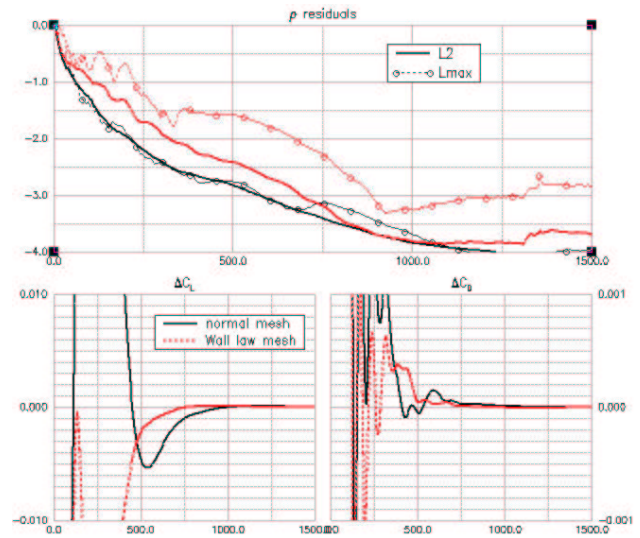takes approximately 6 hours on Fujitsu VPP700 for the fine mesh.

Figure 10 - Compared residuals convergence

Once the calculation is done, it is important to check that the first cell size verifies $20<y_{+1}<200$ as recommended by ONERA [11]. Figure 11 illustrates this surface field on the wing and we can check that the constraint is satisfied correctly.
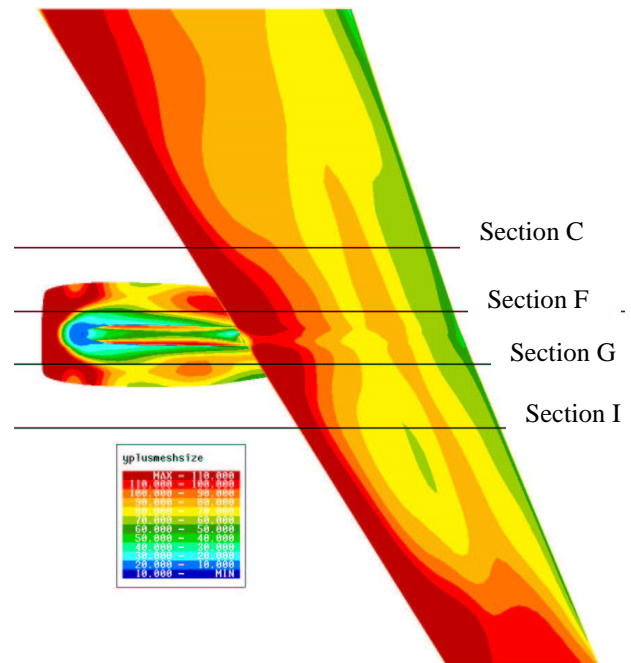

Figure 11 - Wing sections on S3Ch model - wall y^+_1 size

Computed pressure coefficients were plotted in Figure 12 on the four wing sections illustrated in Figure 11 in order to visualize

wing-pylon interactions. The wall law results are very close to those obtained on the refined boundary layer mesh. All physical phenomena such as shock waves and flow accelerations are captured with the same accuracy, specially the strong supersonic acceleration created by pylon interaction on the wing lower surface at inboard pylon side (section F).
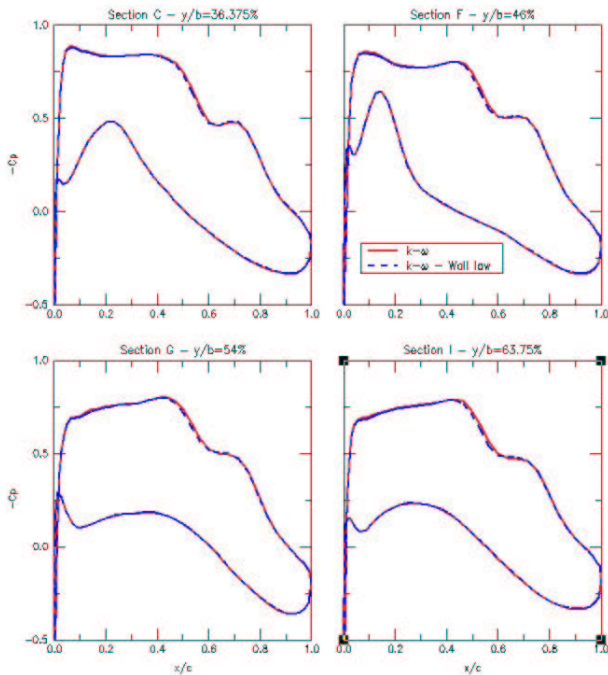

Figure 12 - Wing Cp distribution

Wall law boundary condition treatment has a very slight impact on memory and CPU time consumption. Consequently, an immediate gain can be obtained by the mesh size reduction, that is to say around 25% for the current test case.

3.3.4 Turbulence model effect

Experimental data is available from tests performed in the ONERA S3-Chalais wind tunnel in 1996. Pressure coefficients are available on the four wing sections defined in Figure 11.

Numerical results previously obtained with the k-ω turbulence model (with wall laws) are roughly close to the experimental results but there are two main defects (see Figure 13):

- the shock is located downstream from the experimental position, but it is a well known behavior of the k-ω turbulence model.

- the pressure coefficient peaks on the leading edge upper surface are underestimated.

For these reasons, a new mesh was generated with finer mesh at the leading edge, and new calculations were performed with k-l and Spalart Allmaras turbulence models. As illustrated on Figure 13:

- all turbulence models correctly predict the double compression on the upper surface as well as the strong supersonic acceleration on the pylon inboard side

- shock wave location on the upper surface is very similar between k-l and S.A. calculations and it is now much closer than experimental values.

- leading edge refinement causes a localized flow acceleration on the upper surface, in accordance with experimental trends in sections C and F. However, a discrepancy remains on the level of flow acceleration on the upper surface before the shock compression. This may be explained by wind-tunnel test corrections, which provide equivalent free stream conditions on Mach number and angle-of-attack. A complete calculation should be carried out on the real configuration with upper and lower walls.
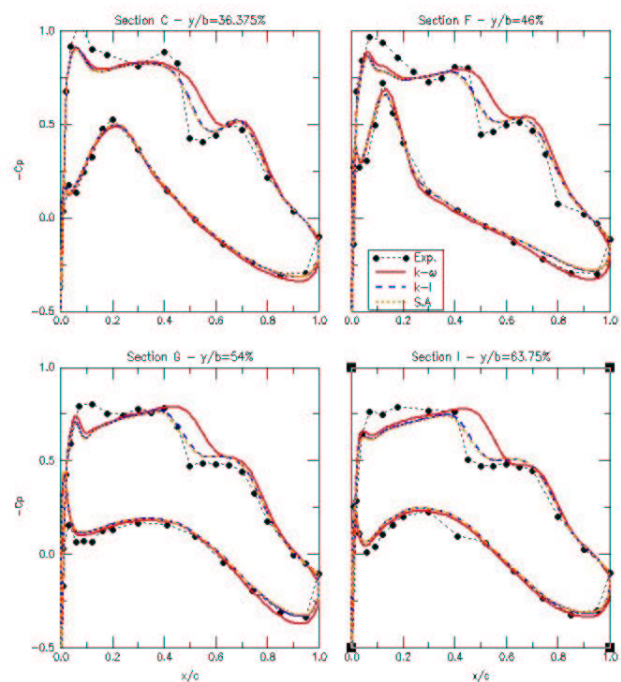

Figure 13 - Turbulence model effect - Experimental data

Conclusion

Through these three industrial applications, we have demonstrated that the elsA code is able to deal efficiently with complex configurations while using advanced functionalities on structured meshes such as Chimera, wall laws and adaptive refinement techniques. Considering the current knowledge, an efficient association of these functionalities can be foreseen in the short term.

The Chimera technique will allow the structured mesh generation time, which is today a real bottleneck in the global CFD process, to be reduced considerably. Wall laws and adaptive refined meshes will allow accurate results to be obtained using much smaller meshes. All in all, it will become easier and faster to study the influence of geometry devices on a reference aircraft (wing tip devices, flap track fairing, strakes…)

In this way we hope to considerably improve the global CFD process efficiency in order to emphasize the use of CFD in the assessment of aerodynamic data.

Acknowledgements

References

[1] L. Cambier and M. Gazaix. "elsA: An Efficient Object-Oriented Solution to CFD Complexity", AIAA 2002-0108, 40th AIAA Aerospace Sciences Meeting and Exhibit, Reno, 2002

[2] Steger J.L., Dougherty F.C., Benek J.A., "A Chimera grid scheme", ASME Mini symposium on advances in grid generation, Houston (USA), June 1993.

[3] Le Pape M.-C., Darracq D., Guillen P., "Design of a Chimera unsteady code, application to store separation" , 7th International symposiun on CFD, Beijing (China), 1997.

[4] C. Benoit and G. Jeanfaivre, "3D Inviscid Rotor and Fuselage Calculations Using Chimera and Automatic Cartesian Partitioning Methods", AHS Aeromechanics 2000, Atlanta, November 2000

[5] Jeanfaivre G., Benoit Ch., Le Pape M.C., "Improvement of the robustness of the Chimera method", AIAA Fluid Dynamics Conference and Exhibit, St-Louis (USA), June 2002.

[6] J.J. Quirk, "An adaptive grid algorithm for computational shock hydrodynamics", Ph.D. thesis, Crandfield Institute of Technology, College of Aeronautics, 1991

[7] M.J. Berger and P. Collela. "Local Adaptive Mesh Refinement for Shock Hydrodynamics", J. Comput. Phys. 82, pp. 67-84, 1989.

[8] JC. Jouhaud. "Méthode d'Adaptation de Maillages Structurés par Enrichissement ", PhD. Thesis, University of Bordeaux I, 1997.

[9] A. Jameson. "Steady State Solutions of the Euler Equations for Transonic Flow by a multigrid Method", Advances in Scientific Comp., pp. 37-70, Academic press 1982.

[10] Chen, H.C. and Patel, V.C., "Near-Wall Turbulence Models for Complex Flows Including Separation", AIAA Journal, vol. 26(6), pp641-648, 1985.

[11] Goncalves E., Houdeville R. "Reassessment of the Wall Functions Approach for RANS Computations", Aerospace Science and Technology, Vol. 5, 2001, pp.1-14

[12] E.V. Laitone, "Comment on "Drag Reduction Factor Due to Ground Effect", Technical Comments. Journal of Aricraft, 1989.

[13] J.Zeihan and X.Zhang. "Aerodynamics of a Single Element Wing in Ground Effect", Journal of Aircraft, Vol.37, N°6, 2000, pp.1058-1064

[14] P.Prel, V. Rivoire, J.Bardou. "Prévision des effets de sol sur un avion de transport commercial", AAAF, 29ème Colloque d'Aérodynamique Appliquée, C.E.L Biscarosse, 1992.

[15] A. Flaig, "Results of Wind Tunnel Ground Effect Measurements on Airbus A320 Using Turbine Power Simulation and Moving Tunnel Floor Techniques", AIAA 90-1427, 16th Aerodynamic Ground Testing Conference, Seattle, 1990.

[16] V.Schmitt, D. Destarac. "Recent progress in drag prediction and reduction for civil transport aircraft at ONERA", AIAA 98-0137, Jan.1998.

[17] S. Amant. "Drag prediction and decomposition, from wake surveys and calculations, in subsonic flows", AIAA 2001-2446, Jun.2001